Multiuser Receiver Architectures for Space Modems

David Bell,* Edgar Satorius,* Igor Kuperman,* and John Koenig†

ABSTRACT. — In this article, we develop multiuser modem architectures suitable for augmentation of existing software-defined flight radios with important near-term enhancements to relay telecom services as well as support for missions requiring entry, descent, and landing (EDL). EDL support for missions like Mars Exploration Rover (MER), Phoenix, Mars Science Laboratory (MSL), and Mars 2020 obtains strong visibility within JPL and NASA headquarters. As part of an agency-wide commitment to support EDL, funding has been made available on past missions to prepare multiple Deep Space Network (DSN) ground station sites, non-DSN ground stations (Greenbank 100-m), and to prioritize in situ coverage from multiple orbiters. Multiuser operations open up new possibilities for simultaneous support of multiple surface landers that are in close proximity such that these surface elements simultaneously appear in the same coverage circle of a single relay orbiter. Simultaneous multiuser support is an important service type for many future surface mission paradigms. In this article, designs for field-programmable gate array (FPGA) implementation of multiuser modems are presented. A fixed-point model of the most promising architecture for space applications is presented as well as simulated performance results based on a fixed-point design that is suitable for FPGA implementation.

I. Introduction

Mars missions will involve communications between multiple assets (e.g., landers, orbiters). Current JPL telecom infrastructure and operations will support some multiuser capabilities through the Deep Space Network (DSN) support of multiple users in a single DSN antenna beam. This study aims to extend these capabilities into the flight radios with important near-term enhancements to relay telecom services as well as support for missions requiring entry, descent, and landing (EDL). EDL support for missions like Mars Exploration Rover (MER), Phoenix, Mars Science Laboratory (MSL), and Mars 2020 obtains strong visibility within JPL and NASA headquarters. As part of an agency-wide commitment to support EDL, funding has been made available on past missions to prepare multiple DSN ground station sites, non-DSN ground stations (Greenbank 100-m), and to prioritize in situ coverage from multiple orbiters.

* Flight Communications Systems Section.
† Flight Electronics and Software Systems Section.

The research described in this publication was carried out by the Jet Propulsion Laboratory, California Institute of Technology, under a contract with the National Aeronautics and Space Administration.

For Phoenix EDL, there were three ground sites and three Mars orbiters providing simultaneous EDL telecom support. In the case of the in situ orbiters, each individual orbiter has been capable of single-mode support, for example, direct data demodulation of EDL data or open-loop record of the EDL signal spectrum. The low data rates associated with EDL event reporting suggest that an individual flight radio could provide simultaneous demodulation, open-loop recording, and Doppler radiometric services. This multimode EDL support would effectively double EDL telecom redundancy relative to our current single-mode per spacecraft support approach, and result in dramatic risk reduction and potential cost reductions for EDL support. Furthermore, the multiuser design can easily accommodate operational scenarios wherein MSL uses adaptive data rates (ADR), 64 ksps to 4096 ksps, and InSight (planned for 2016) uses a fixed rate of 512 kbps, with both relaying data through the Mars Reconnaissance Orbiter (MRO). In general, landers separated by less than 1250 km or 21 deg along any great circle will have some simultaneous coverage from MRO. This scenario is depicted in Figure 1.

Beyond this, multimode operations open up new possibilities for simultaneous support of multiple surface landers that are in close proximity such that these surface elements simultaneously appear in the same coverage circle of a single relay orbiter. This will be the case with cooperative lander missions, a lander–rover operations pair, distributed intelligent lander missions, and future deployment of multiple equipment components for support of complex sample return or manned operations. In short, simultaneous multiuser support is an important service type for many future surface mission paradigms.

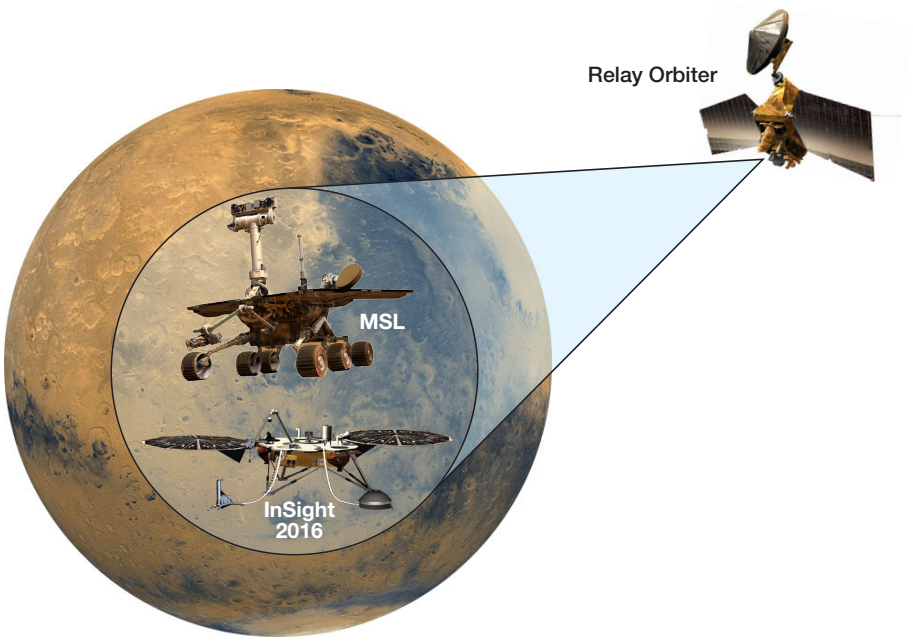

Figure 1. Multiuser scenario: MSL and InSight relaying data through MRO.

This article presents the results of a study carried out to assess the potential adaptation of the Electra radio to a multiuser scenario. The basic concept is a frequency-division multiple access (FDMA) communications scheme wherein different users occupy nonoverlapping signal bands all lying within the receiver's intermediate frequency (IF) bandwidth. In carrying out this development, several modem architectures were considered [1]: (1) multiple IF slices/analog-to-digital converters (ADCs)/field-programmable gate arrays (FPGAs), each programmed with an Electra baseband modem; (2) common IF but multiple ADCs and FPGAs; and (3) common IF, single ADC, and single or multiple FPGAs programmed to accommodate the FDMA signals. These options represent the usual trade-off between analog and digital complexity. Given the space application, a common IF is preferable; however, multiple users present dynamic range challenges (e.g., near–far constraints) that would favor multiple IF slices (option 1). Vice versa, with a common IF and multiple ADCs (option 2), individual automatic gain control (AGC) of the ADCs would be an important consideration. Option 3 would require a common AGC control strategy to prevent ADC saturation and would entail multiple digital downconversion paths within the FPGA.

In this article, an overview of the different Electra design options considered will be presented in Section II and the most promising design will be evaluated in terms of fixed-point simulation analysis in Section III. In particular, signal channel spacing as a function of user data rates and transmit powers will be evaluated. In addition, the results of a current FPGA development of a dual-user modem on a Xilinx Virtex-2 FPGA (XC2V3000) will be presented in Section IV, including resource utilization estimates. The Virtex-2 is being used in the Electra modem currently on both the Mars Atmosphere and Volatile Evolution (MAVEN) mission and the Trace Gas Orbiter (TGO) mission [2]. Finally, conclusions are presented in Section V.

II. Multiuser Modem Architectures

Within the family of common IF multiuser modem architectures, the options depicted in Figure 2 (illustrated for dual users) have been considered. For all options, dual digital channels (demodulators) are required. However, for Option 2(a), dual analog channels are also required and thus this option is not considered further. Options 2(b) and 2(c) only require a single analog channel with dual digital channels. Option 2(b) combines digital and analog AGC control. However, this option does not guarantee that the root-mean-square (RMS) inputs to the dual digital tracking loops (within the digital demods) are equalized. Consequently, we have focused on Option 2(c), which employs a single wideband AGC to prevent ADC saturation and additional digital AGC loops to regulate the bandwidths of the digital tracking loops. Note that this architecture is more robust to the strong–weak input signal scenario as the wideband front-end AGC avoids ADC saturation by the strong signal.

In addition, for Option 2(c), we have introduced a multichannel digital downconversion front-end that is motivated by polyphase filter bank theory [3,4]. The downconverter architecture is shown in Figure 3 including the dual-channel version, which is currently being implemented. The filters shown in Figure 3, $H_k(z)$, provide the channel isolation. These polyphase filters are derived by subsampling (by M) a real, prototype lowpass filter. The sampling rate for each output channel Y_k is F_s/M, where F_s is the input ADC sampling rate.

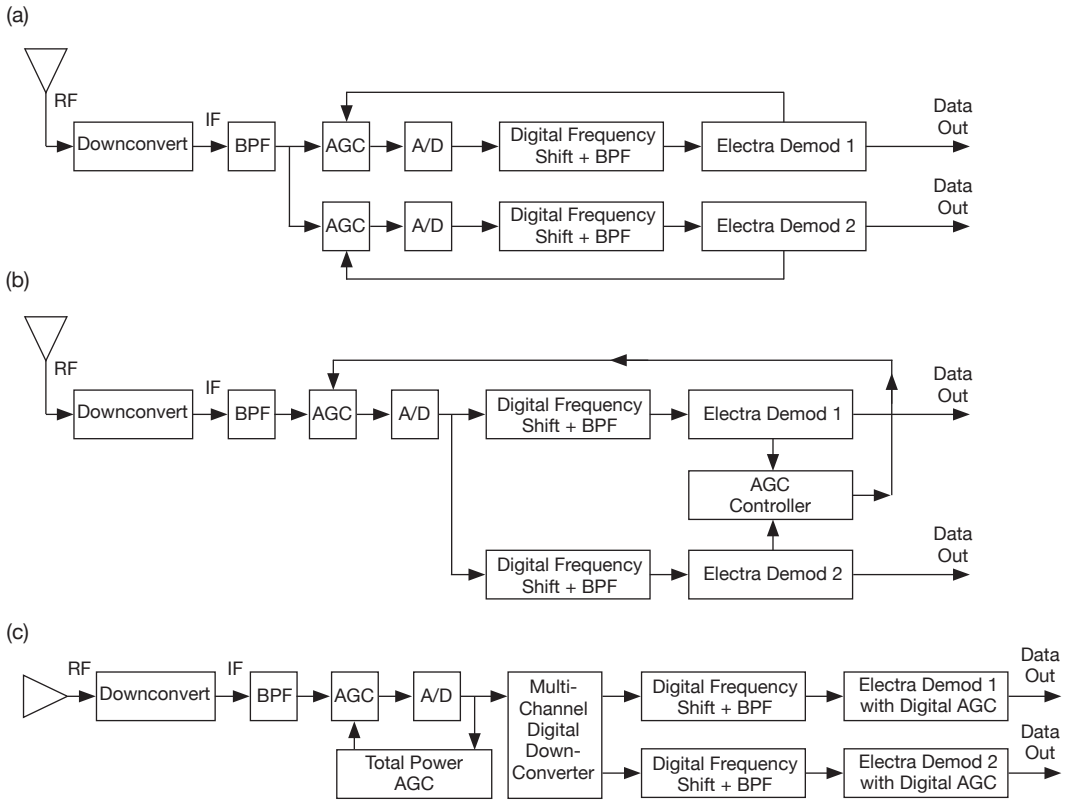

Figure 2. Common IF dual-user modem architectures: (a) dual analog/digital channels and low-resolution ADCs with dual AGC control; (b) dual digital channels with a high-resolution ADC and single AGC control; (c) dual digital channels with a high-resolution ADC and single AGC control plus dual digital AGC control.

For the dual-user downconverter — Figure 3(b) — the $H_k(z)$ are typically 16 tap finite impulse response (FIR) filters. Note also for the dual-user downconverter that since the input (ADC output) is real, then the outputs Y_1 and Y_2 are also real.

Sample dual-user spectra at the output of the ADC and the dual-channel downconverter are shown in Figure 4, corresponding to an Electra/MRO configuration wherein the ADC sample rate is F_s = 76.72322224/4 ~19.18 MHz and the IF bandwidth is ~8 MHz. For purposes of illustration, spectra are shown for two users, both transmitting suppressed carrier binary phase-shift keying (BPSK) modulation at 512 kbps and 1024 kbps. As seen from Figure 4(a), Δf denotes the separation of either carrier from the half-Nyquist frequency $F_s/4$ ~4.8 MHz and thus $2\Delta f$ is the separation between the two carriers. For the example shown in Figure 4, there is a 4 MHz separation between carriers.

At the outputs of the dual-channel downconverter — Y_1 and Y_2 in Figure 3(b) — the spectra are centered at the same frequency: $F_s/4 - \Delta f$ ~2.8 MHz. Thus, additional frequency translation is required to center the carriers at baseband. This is the function of the digital frequency shift + bandpass filter (BPF) blocks in Figure 2(c). These blocks are simplified due to the common center frequency. A block diagram for the digital frequency shifters/bandpass filters (complex basebanders) is shown in Figure 5.

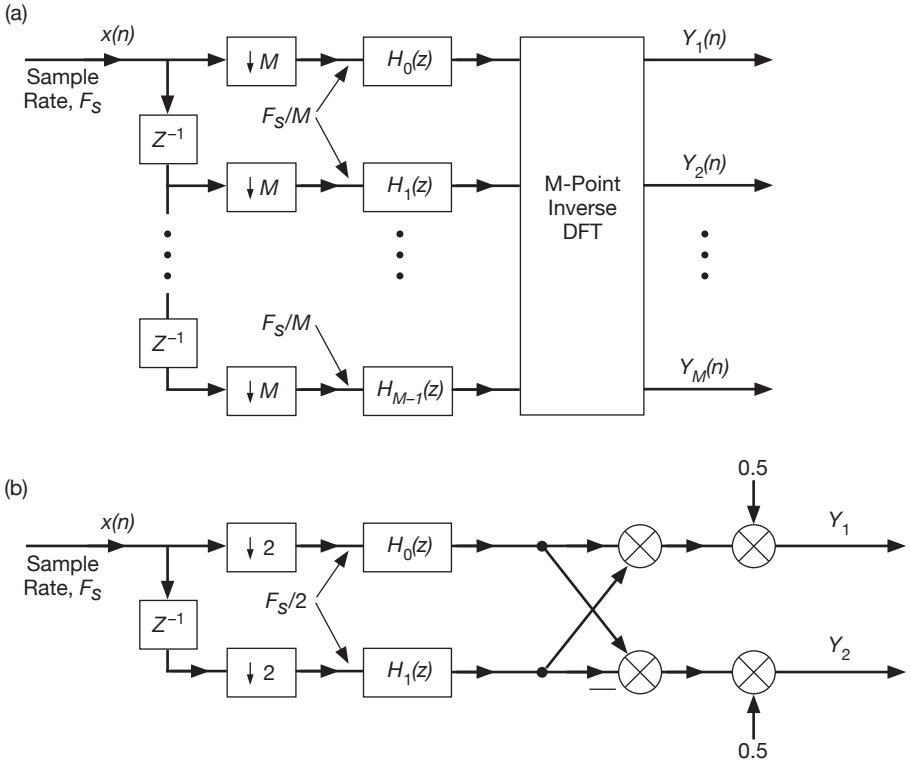

Figure 3. Multichannel digital downconverter architectures: (a) *M*-channel; (b) dual channel.

As seen in Figure 5, the basebander comprises two multipliers per user but just a single numerically controlled oscillator (NCO). The NCO, which is clocked at $F_s/2$, accumulates the common center frequency $F_s/4 - \Delta f$ normalized by $F_s/2$, i.e., $f_0 = (F_s/4 - \Delta f)/(F_s/2) = 0.5 - 2\Delta f/F_s$. The NCO then outputs the cosine and sine (nco_real and nco_imag, respectively, in Figure 5) of the accumulated phase, which multiplies the real inputs, Y_1 and Y_2 in Figure 3(b). The outputs from the multiplies are then filtered by the lowpass (half-band) FIR filter, $h_{HB}(n)$. The purpose of these lowpass filters is to remove images created by the multiplies. The outputs, denoted by I_k and Q_k in Figure 5, are then the real and imaginary parts of the complex baseband outputs, $Z_k (k = 1, 2)$. This complex basebander is part of the current Electra modem design [5], though the NCO in Electra is much simpler inasmuch as the single-user spectrum is centered at the half-Nyquist frequency $F_s/4$ after the ADC and thus the NCO reduces to multiplies by ±1.

Examples of four-user spectra at the output of the ADC and the four-channel downconverter are shown in Figure 6, again corresponding to an Electra/MRO configuration. For this case, all four users are transmitting suppressed carrier, BPSK modulation with the transmitted data rates 128 kbps, 256 kbps, 512 kbps, and 1024 kbps, and data carrier frequencies located within the ADC Nyquist band at Δf, $F_s/4 \pm \Delta f$, and $F_s/2 - \Delta f$: see Figure 6(a). With these carrier placements, all four carrier frequencies are the same (at Δf) in the outputs of the downconverter as seen in Figure 6(b).

Note also that not all of the carriers are equally spaced within the Nyquist band. For the example shown in Figure 6 ($\Delta f = 1.4$ MHz), the 1024 and 512 kbps data carriers are separated by $2\Delta f = 2.8$ MHz, whereas the 128 and 1024 kbps data carriers are separated by

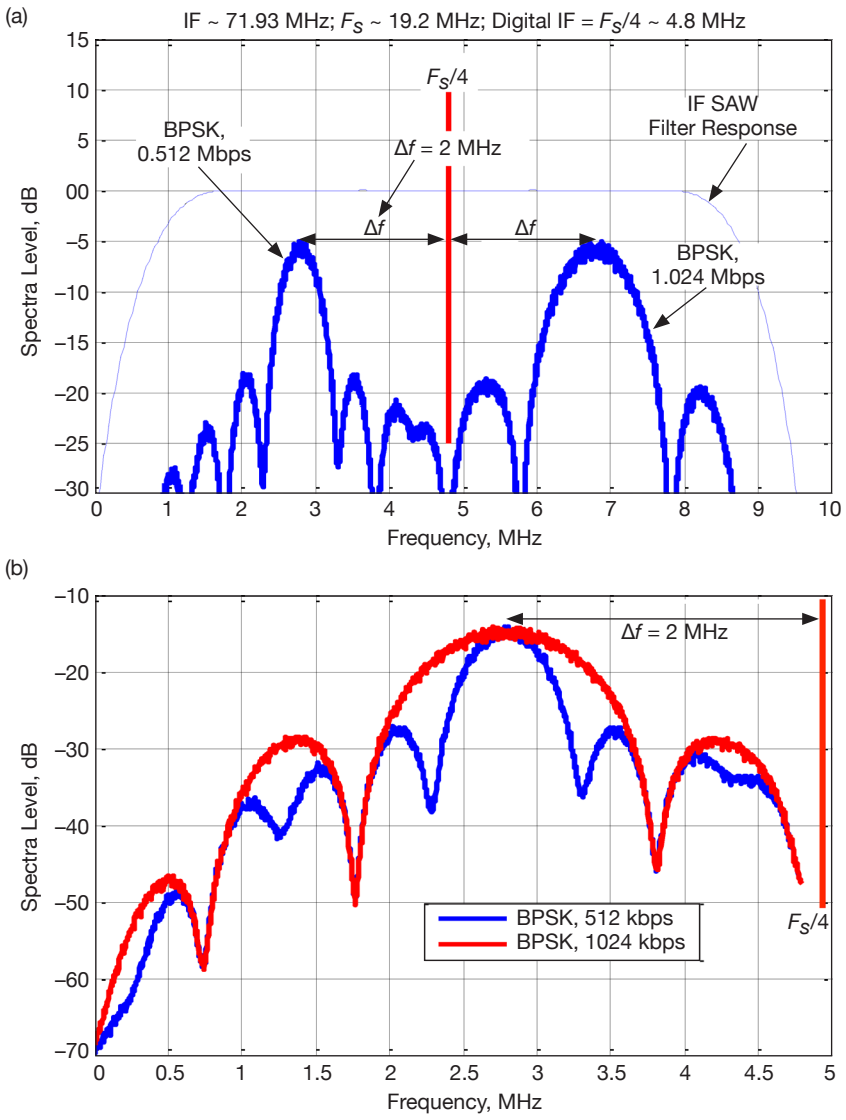

Figure 4. Dual-user spectra: (a) at the ADC output; (b) dual-channel output spectra.

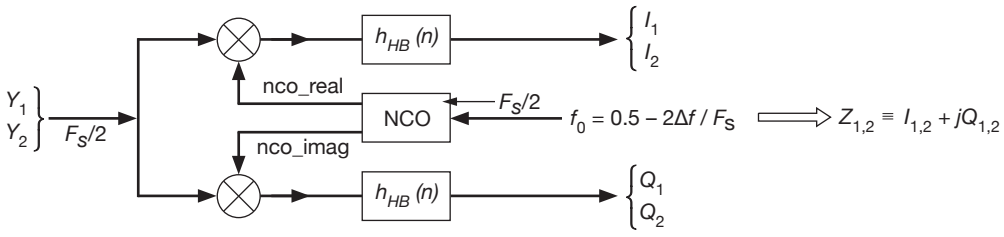

Figure 5. Dual-user complex basebander.

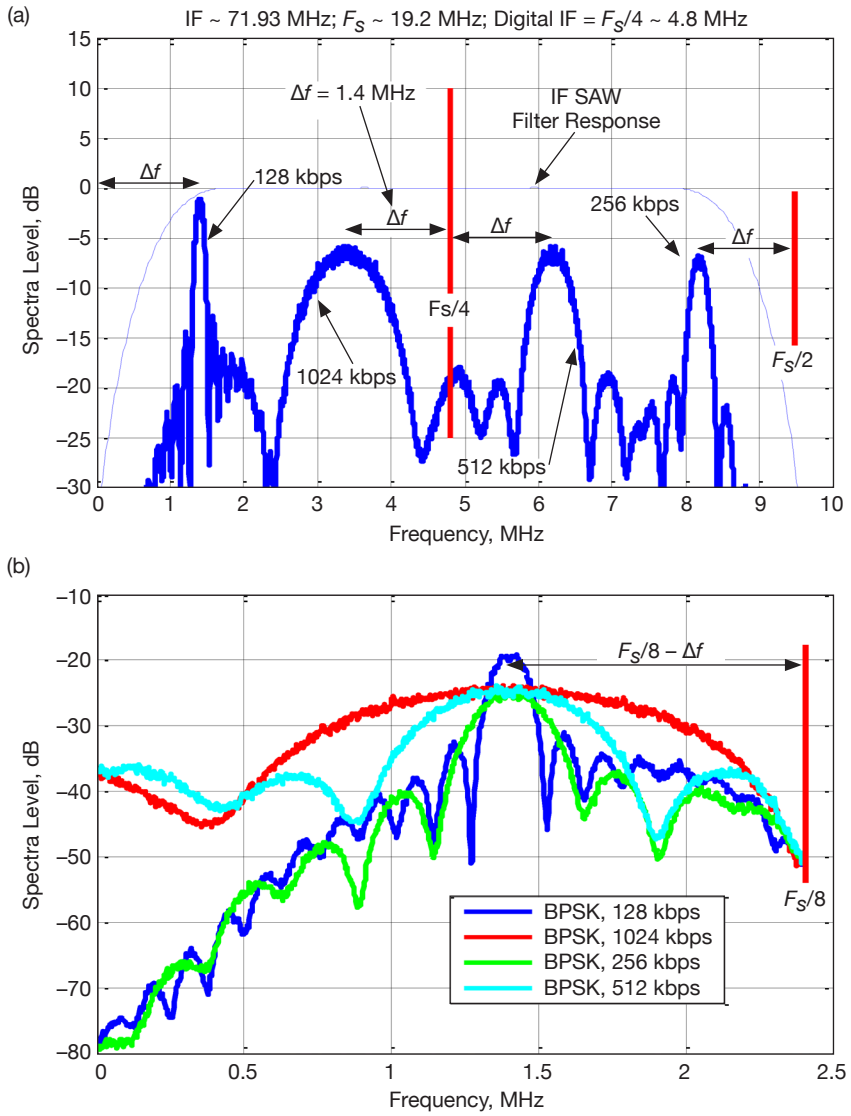

Figure 6. Four-user spectra: (a) at the ADC output; (b) four-channel output spectra.

$F_s/4 - 2\Delta f \sim 2$ MHz (similarly for the 512 and 256 kbps carriers). However, the carriers can be equally spaced by setting $\Delta f = F_s/16 \sim 1.2$ MHz. Thus, there is considerable flexibility in choosing the data carrier frequencies such that all four carrier frequencies are the same in the downconverter outputs. This simplifies the four-channel complex basebander design in that only one NCO is required, as shown in Figure 7. Note that two of the four downconverter output channels, Y_2 and Y_4, are complex and, in fact, are complex-conjugate pairs.

As indicated in Figure 7, the four-user complex basebander comprises four (generally complex) multipliers but a single NCO. The NCO, which is now clocked at $F_s/4$, accumulates the common center frequency $F_s/8 - \Delta f$ normalized by $F_s/4$, i.e., $f_0 = (F_s/8 - \Delta f)/(F_s/4) = 0.5 - 4\Delta f/F_s$. The NCO then outputs nco_real and nco_imag, which multiplies the downconverter outputs, Y_k. The outputs from the multiplies are then filtered by the lowpass (half-band) FIR filter, $h_{HB}(n)$. The outputs, Z_k, are the desired complex baseband outputs.

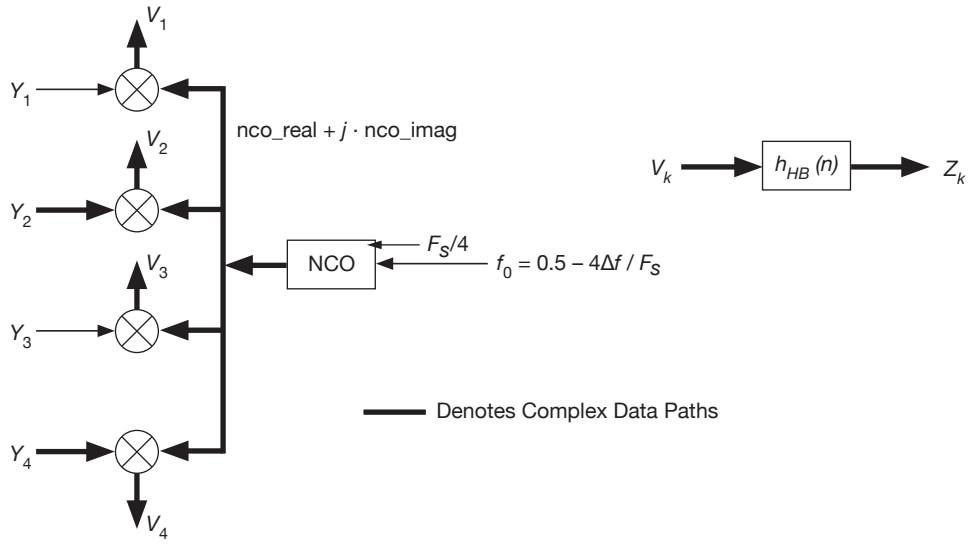

Figure 7. Four-user complex basebander.

Section IV. Dual-User Simulated Performance Analysis and Implementation Considerations

We have conducted numerous fixed-point Matlab simulation experiments for purposes of evaluating the performance of the quantized, dual-user modem. With reference to Figure 2(c), data paths through the downconverter and complex basebanders are predominantly 8 bits wide, as indicated in Figure 8, where the fixed-point, front-end model for the dual-user modem is shown. The wordlengths for the various data paths in Figure 8 are indicated by the notation <B,I,t>, where B denotes the total number of bits (including sign, integer, and fractional bits), I denotes the number of integer bits, and t denotes two's complement representation. The remainder of the dual-user modem basically duplicates the Electra demodulator as implemented for the MAVEN and TGO missions.

Sample bit-error rate (BER) curves are shown in Figure 9 corresponding to different data rate pairs for each user: (i) 1024/1024 kbps; (ii) 512/1024 kbps; (iii) 512/512 kbps, and (iv) 256/256 kbps. In all cases, the modulation is suppressed-carrier BPSK and the data carrier separation between users is $2\Delta f = 2$ MHz. With reference to Figure 4(a), User 1 is positioned on the high side and User 2 is on the low side. Thus, for example, the ADC output spectrum for case (ii) would comprise the high-rate user on the low side and the low-rate user on the high side — the exact opposite of the ADC spectrum shown in Figure 4(a).

With reference to Figure 4(a), we see the possibility for significant adjacent channel interference (ACI) as Δf reduces to 1 MHz. This is clearly observed in Figure 9, where significant BER degradation is seen, especially for the higher-data-rate pairs (cases i and ii). The difference between the different user BERs in Figures 9(a) and 9(b) directly depends on the user's data rate and the amount of ACI.

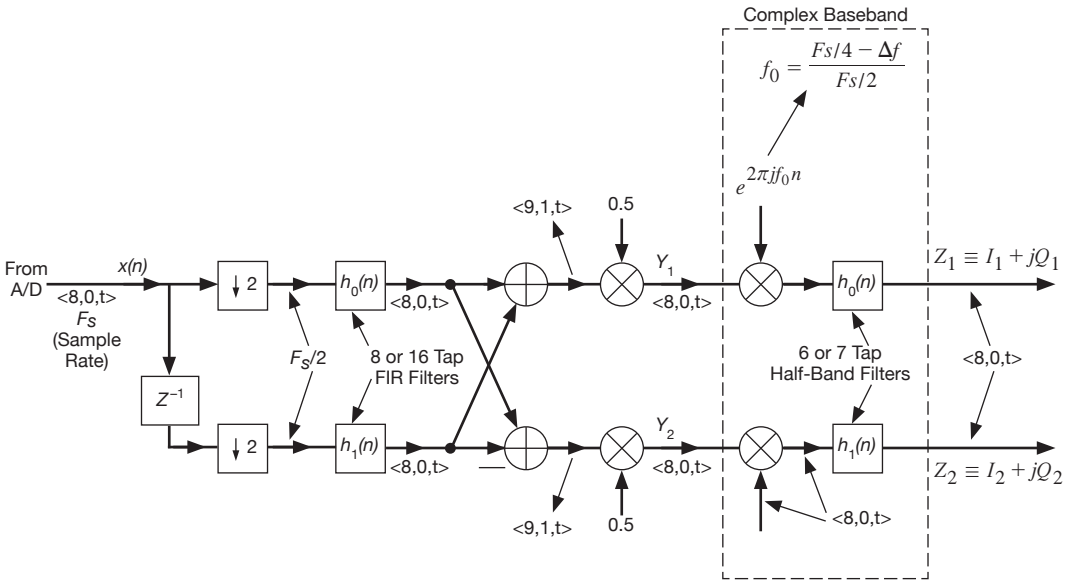

Figure 8. Dual-user downconverter/complex basebander fixed point model.

For example, consider case (ii) wherein the BER performance for User 1 at 512 kbps is shown in Figure 9(a) when the E_sN_0 for User 2 at 1024 kbps is maximum (9 dB). Clearly, the wider sidelobes of User 2 will create ACI for the lower-data-rate User 1; however, this is offset by the reduction in the number of samples/symbol for the higher-data-rate User 2 (approximately 9 samples/symbol versus approximately 19 samples/symbol for the lower-data-rate User 1), thereby leading to more degradation for User 2. This is observed by comparing Figures 9(a) and 9(b). It is seen that the BER performance for the 1024-kbps user, Figure 9(b), is somewhat worse due to fewer samples/symbol as well as the ACI from User 1.

As the data rates decrease for each user, cases (iii) and (iv), performance improves due to less ACI — for cases (iii) and (iv) approximately 19 samples/symbol are used by both users. Alternatively, instead of decreasing the user data rates, increasing the carrier separation improves BER performance for all the cases (i)–(iv). This is clearly evident in Figure 10(a) and Figure 10(b), where the carrier separation has been increased to $2\Delta f = 4$ MHz. Now ACI becomes less of an issue for any of the data pairs and correspondingly BER degradation is reduced.

It should be noted that there was no attempt to optimize receiver (loop) parameters for the different cases shown in Figures 9 and 10. In particular, a single set of loop parameters was used in all cases wherein the carrier tracking loop bandwidths were matched but the symbol tracking loop bandwidths were different. This is why, for example, in cases (iii) and (iv) the BER performance for Users 1 and 2 differ at high E_sN_0 (Figures 9 and 10).

Given the results of this performance analysis as well as the desirability for simultaneous user operation as discussed in Section I, we have initiated an FPGA design and implementation of a dual-user modem based on the Xilinx Virtex-2 FPGA (XC2V3000) that is being used in the Electra modem currently on both MAVEN and TGO. As the first step toward the

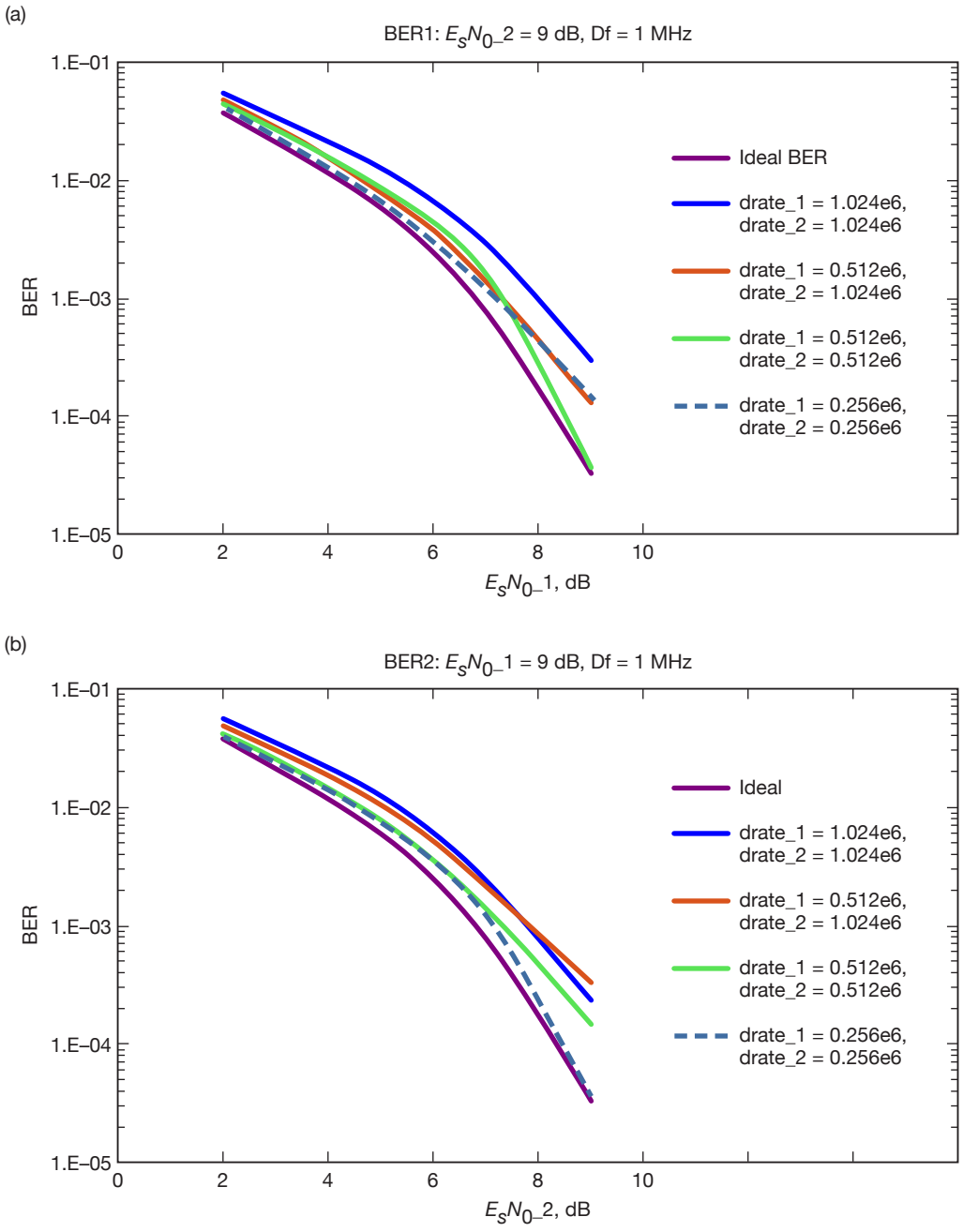

Figure 9. Dual-user BER simulations with Δf = 1 MHz: (a) User 1; (b) User 2.

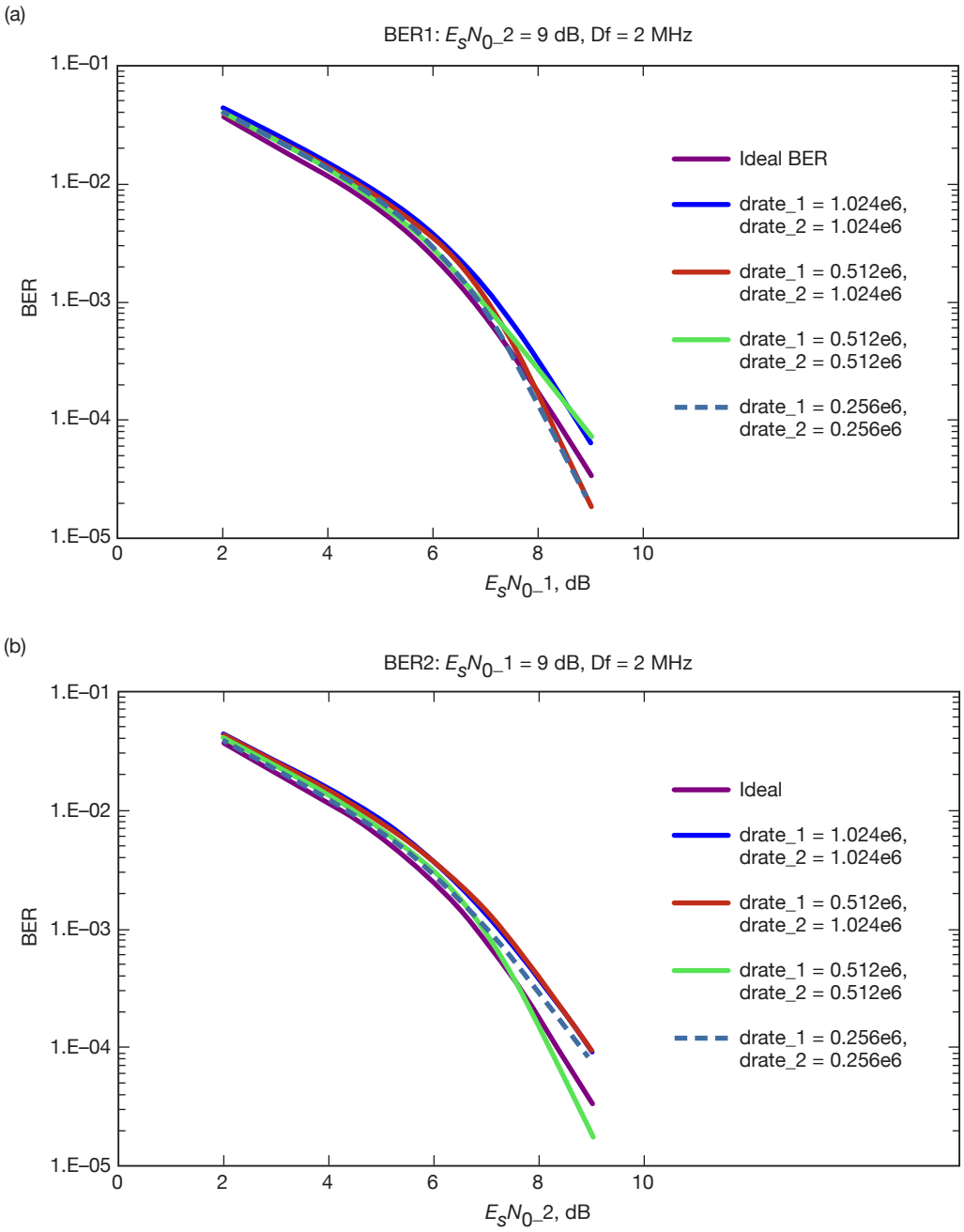

Figure 10. Dual-user BER simulations with $\Delta f = 2$ MHz: (a) User 1; (b) User 2.

development of an FPGA dual-user modem, we have carried out a preliminary analysis of the Virtex-2 based on both look-up table (LUT) and flip-flop (FF) utilization. The Virtex-2 has a total of 28,672 LUTs and 28,672 FFs available for use. In addition, the Virtex-2 has 96 embedded multipliers as well as 1728 kbits of block random-access memory (RAM).

Figure 11 shows the projected LUT and FF utilization analysis for the dual-user modem, including partitioning of each receiver channel (Receivers 1 and 2) into its constituent components (tracking loops, etc.). Additional functions including control registers and transmitter buffers are included in the Receiver 1 allocation and the Common partition includes the modulators as well as test interfaces and top-level glue logic. Also, this utilization estimate does not include the channel decoders (assumed to be implemented in a separate dedicated module) and the second receive channel does not support radiometric data collection or real-time clock time tagging.

As indicated in Figure 11, the dual-user modem is estimated to utilize almost all of the Virtex-2 FPGA (with only 5 percent unused LUTs). Nevertheless, this partitioning is based on an architecture that will provide functioning dual-user demodulator capability in a space environment. Furthermore, since this analysis is based on the Virtex-2, the resulting firmware can be directly uploaded to MAVEN and/or TGO to enable a dual-user capability. Also, efficient utilization of the embedded multipliers will further free up the LUT utilization.

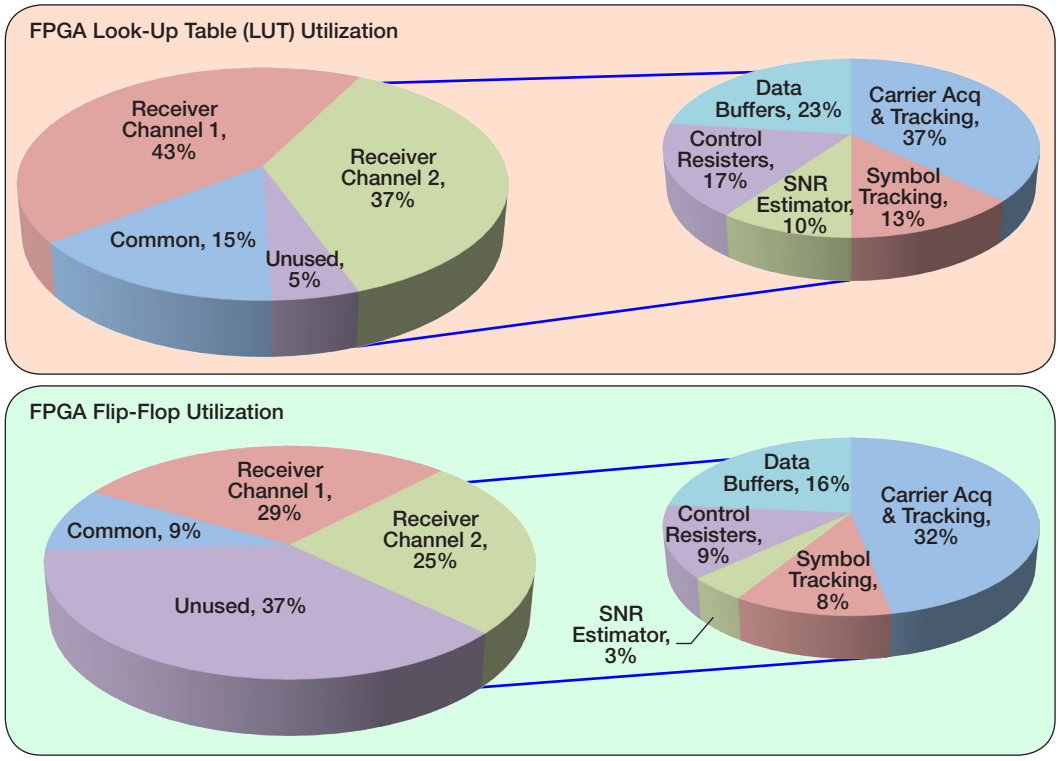

- "Receiver Channel 1" includes additional common control registers and the transmit data buffers.
- "Common" consists of the modulator, test interfaces, and top-level glue logic.

Figure 11. Dual-user utilization with Xilinx Virtex-2.

Section V. Conclusions

In this article, we have identified a dual-user modem architecture, Figure 2(c), which can be implemented on the Xilinx Virtex-2 FPGA (XC2V3000) that is being used in the Electra modem currently on both MAVEN and TGO. Based on the results presented in Section IV, it is seen that this architecture provides reliable dual-user communications and is thus a good candidate for demonstration and implementation.

Given the results from this study, the next step is to conduct prototype demonstrations using a Space Communications and Navigation (SCaN) Testbed FPGA development board (Xilinx Virtex-2 with an ADC clocked at 49.244 MHz) or the Universal Space Transponder (UST) FPGA development board (Xilinx Virtex-4 with an ADC clocked at 150 MHz). The latter has plenty of room, with 178,176 LUTs and FFs available, and would thus enable an easier implementation and demonstration. The former, however, would be representative of the actual firmware environment on MAVEN and TGO and would thus be critical in reducing the risks for future software uploads to these missions and furthermore would pave the way for a flight demonstration with the SCaN testbed on the International Space Station.

References

[1] E. Satorius, B. Shah, K. Bruvold, and D. Bell, "Adaptation of the Electra Radio to Support Multiple Receive Channels," *Proceedings of the 2011 IEEE Aerospace Conference*, pp. 1–10, Big Sky, Montana, March 5–12, 2011.

[2] C. Edwards, B. Arnold, D. Bell, K. Bruvold, R. Gladden, P. Ilott, and C. Lee, "Relay Support for the Mars Science Laboratory and the Coming Decade of Mars Relay Network Evolution," *Proceedings of the 2012 IEEE Aerospace Conference*, pp. 1–11, Big Sky, Montana, March 3–10, 2012.

[3] R. Sadr, P. P. Vaidyanathan, D. Raphaeli, and S. Hinedi, *Parallel Digital Modem Using Multirate Digital Filter Banks*, JPL Publication 94-20, Jet Propulsion Laboratory, Pasadena, California, August 1994.

[4] M. Srinivasan, C.-C. Chen, G. Grebowsky, and A. Gray, "An All-Digital, High Data-Rate Parallel Receiver," *The Telecommunications and Data Acquisition Progress Report*, vol. 42-131, Jet Propulsion Laboratory, Pasadena, California, pp. 1–16, November 15, 1997.
http://ipnpr.jpl.nasa.gov/progress_report/42-131/131K.pdf

[5] E. Satorius, T. Jedrey, D. Bell, A. Devereaux, T. Ely, E. Grigorian, I. Kuperman, and A. Lee, "The Electra Radio," Chapter 2 in *Autonomous Software-Defined Radio Receivers for Deep Space Applications*, J. Hamkins, M. Simon, J. Yuen, eds., Wiley-Interscience, October 13, 2006. Available electronically: Deep-Space Communications and Navigation Series, Jet Propulsion Laboratory, Pasadena, California, 2006.
http://descanso.jpl.nasa.gov/Monograph/series9/Descanso9_02.pdf